

# Extrinsic analysis on manifolds is computationally faster than intrinsic analysis with applications to quality control by machine vision

R. N. Bhattacharya<sup>a</sup>, L. Ellingson<sup>b</sup>, X. Liu<sup>b</sup>, V. Patrangenaru<sup>b,\*†</sup> and M. Crane<sup>c</sup>

In our technological era, non-Euclidean data abound, especially because of advances in digital imaging. Patrangenaru ('Asymptotic statistics on manifolds', PhD Dissertation, 1998) introduced extrinsic and intrinsic means on manifolds, as location parameters for non-Euclidean data. A large sample nonparametric theory of inference on manifolds was developed by Bhattacharya and Patrangenaru (*J. Stat. Plann. Inference*, 108, 23–35, 2002; *Ann. Statist.*, 31, 1–29, 2003; *Ann. Statist.*, 33, 1211–1245, 2005). A flurry of papers in computer vision, statistical learning, pattern recognition, medical imaging, and other computational intensive applied areas using these concepts followed. While pursuing such location parameters in various instances of data analysis on manifolds, scientists are using intrinsic means, almost without exception. In this paper, we point out that there is no unique intrinsic analysis because the latter depends on the choice of the Riemannian metric on the manifold, and in dimension two or higher, there are infinitely such nonisometric choices. Also, using John Nash's celebrated isometric embedding theorem and an equivariant version, we show that for each intrinsic analysis there is an extrinsic counterpart that is computationally faster and give some concrete examples in shape and image analysis. The computational speed is important, especially in automated industrial processes. In this paper, we mention two potential applications in the industry and give a detailed presentation of one such application, for quality control in a manufacturing process via 3D projective shape analysis from multiple digital camera images. Copyright © 2011 John Wiley & Sons, Ltd.

**Keywords:** extrinsic and intrinsic analysis; directional data analysis; shape analysis of planar closed curves; Kendall's shape spaces; statistical size-and-shape analysis; 3D-projective shape analysis; nonparametric inference; quality control; machine vision

## 1. Data analysis on non-Euclidean, locally Euclidean spaces

### 1.1. Data on manifolds

Multivariate data are data on a flat (zero curvature) finite dimensional manifold. Other examples include directional data, shape data, medical imaging data, protein data, visual data for quality control of manufacturing processes, astronomy data, geology data, and pattern recognition data. Ultimately, almost any numerical data problem can be expressed as data analysis on manifolds or on sample spaces that admit a manifold stratification. Examples of data on manifolds are shown in Figure 1. Given on the top row are examples of medical imaging data: an X-ray image of a human skull with marked anatomical landmarks, a computer tomography scan, a slice of a diffusion tensor imaging signal of a brain, and a photograph of a portion of the interior of an eye. On the bottom row, from left to right, we display wind direction, contour data of a pear and a hand gesture, a digital camera image, and an aerial image. Modern nonparametric analysis of data on

<sup>a</sup>University of Arizona, Tucson, AZ, USA

<sup>b</sup>Florida State University, Tallahassee, FL, USA

<sup>c</sup>Office of Research and Development, US Environmental Protection Agency, Cincinnati, Ohio

\*Correspondence to: V. Patrangenaru, Florida State University, Tallahassee, FL, USA.

†E-mail: vic@stat.fsu.edu

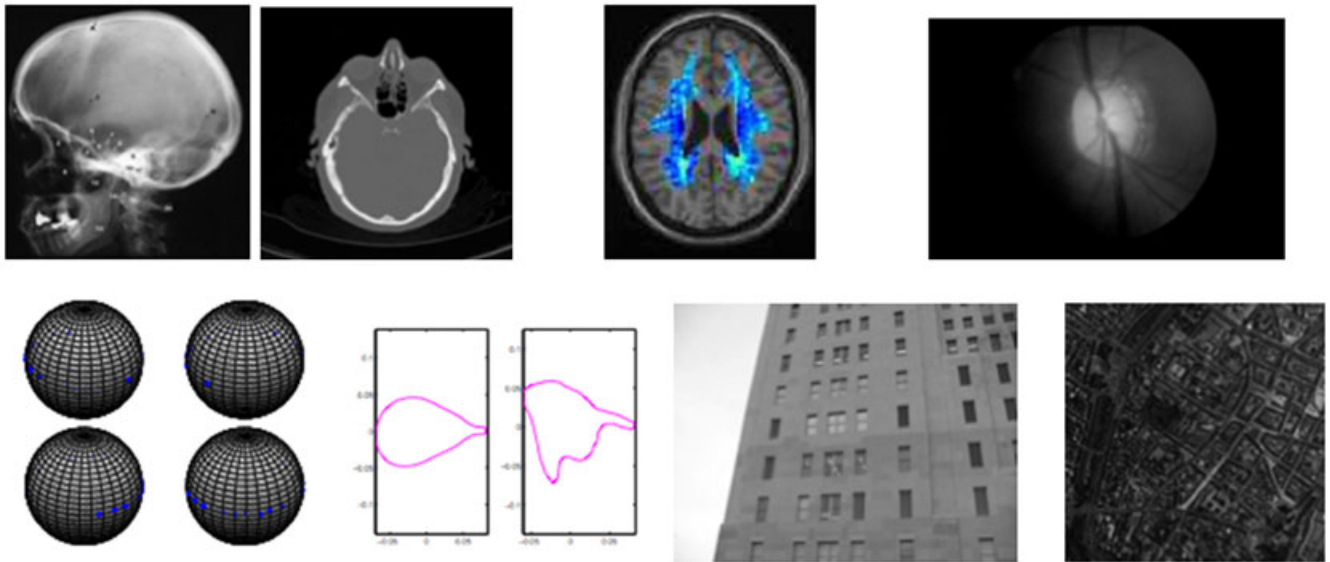


Figure 1. Examples of data on manifolds from medical imaging, from meteorology, and from pattern recognition.

manifolds was built on ideas of central figures of mathematicians and statisticians. The people who paved the way to this modern, vibrating research domain are listed in Figure 2, a distinguished sample in the history of mathematical sciences.

1.2. Manifolds, random objects, and their Fréchet statistics

A topological manifold of dimension  $p$  is a metric space  $(\mathcal{M}, \rho)$  that is locally homeomorphic to the Euclidean space  $\mathbb{E}^p = (\mathbb{R}^p, \|\cdot\|_0)$ . The set of all these local homeomorphisms  $(U, \varphi), \varphi : U \rightarrow \varphi(U) \subseteq \mathbb{R}^p$  is a topological atlas of the manifold. As an example, a planet’s surface may be thought of as a 2D manifold that looks like a sphere with many handles on it. Such a handle is displayed in Figure 3. Einstein and other physicists regard the space–time continuum as a 4D manifold. Statisticians were earlier led to the analysis of manifold-valued data in dealing with directional and axial statistics (see, e.g., [1–3]) and later developed important tools for shape analysis [4–7]).

Given a separable metric space  $(\mathcal{M}, \rho)$ , we consider the  $\sigma$ -field  $\mathcal{B}_{\mathcal{M}}$  generated by open balls in  $(\mathcal{M}, \rho)$ . Assume that  $(\Omega, \mathcal{A}, P)$  is a probability space. A random object (r.o.) on the complete, separable metric space  $(\mathcal{M}, \rho)$  is a function  $X : \Omega \rightarrow \mathcal{M}$ , such that if  $G \in \mathcal{B}_{\mathcal{M}}$ , then  $X^{-1}(G) \in \mathcal{A}$ . The Fréchet function associated with an r.o.  $X$  on  $\mathcal{M}$  is

$$F_{\rho}(x) = E(\rho^2(x, X)). \tag{1}$$

The minimum of the Fréchet function, the least expected squared distance to a point on  $\mathcal{M}$ , is the Fréchet total variance of  $X$ , say  $F_{\rho}(x) = t \Sigma_{X, \rho}$ , and the set of all minimizers of  $F_{\rho}$  is the Fréchet mean set. If the Fréchet mean set has a unique minimizer, this minimizer  $\mu = \mu_{X, \rho}$  is called the Fréchet mean of  $X$  [8]. There is no known condition for the existence of the Fréchet mean of an arbitrarily spread r.o. on a complete separable metric space.

If  $X_1, \dots, X_n$  are i.i.d. r.o.’s from a probability distribution on  $(\mathcal{M}, \rho)$ , the total sample Fréchet variance and the sample Fréchet mean set are, respectively, the total Fréchet variance and the Fréchet mean set of the empirical distribution

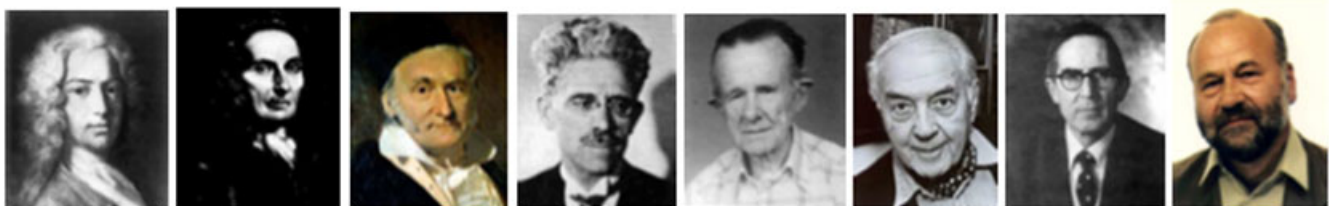


Figure 2. D. Bernoulli, A. deMoivre, K. F. Gauss, M. Fréchet, H. Cramer, G. Watson, D. G. Kendall, and H. Ziezold.



Figure 3. The Delicate Arch in Utah, USA: the geoid surface is a handle body.

$$\hat{Q}_n = \frac{1}{n}(\delta_{X_1} + \cdots + \delta_{X_n}).$$

The consistency of the Fréchet sample mean set, as an estimator of the Fréchet mean set, is essentially due to H. Ziezold [9] with a strengthening and a detailed proof due to Bhattacharya and Patrangenaru [10]. Note that for arbitrary separable complete metric spaces, there are no results on asymptotic distributions of Fréchet sample means because one requires the use of differential calculus on the sample space  $(\mathcal{M}, \rho)$  for this purpose. The most general class of separable metric spaces on which one may differentiate is the class of differentiable manifolds. A manifold has a differentiable structure if it admits an atlas  $\mathcal{U}$ , with the property that for any pair of charts  $((U, \varphi) \in \mathcal{U}, (V, \psi) \in \mathcal{U})$ , the *transition maps*  $\varphi \circ \psi^{-1} : \psi(U \cap V) \rightarrow \varphi(U \cap V)$  are differentiable. For simplicity, we assume that the transition maps are of class  $C^\infty$ .

Those manifolds arising as sample spaces are smooth, including  $\mathbb{R}^p$  for multivariate analysis and the spheres  $S^{p-1}$  for directional data analysis. Certain Lie groups, such as the special orthogonal groups for analysis of data on the movement of tectonic plates and the group of positive definite symmetric matrices for analysis of DTI data analysis, also fall into this category. Additionally, real and complex Grassmann manifolds arise for the analysis of affine shape spaces and Kendall's similarity shape spaces and in signal tracking problems, whereas products of real projective spaces are found in projective shape analysis.

The asymptotic distribution of the Fréchet sample means for a random sample from a probability measure on a smooth manifold was derived by Bhattacharya and Patrangenaru [11]. Computations of Fréchet sample means for a given distance are, in general, based on iterative algorithms, making estimation of Fréchet means time consuming.

## 2. Extrinsic and intrinsic geometry of a manifold

For in-depth information regarding the machinery of differential geometry, such as differential functions between manifolds, curves on manifolds, tangent spaces, tangent bundles, the differential of a differentiable function, immersions, embeddings, vector fields, tensor fields, partitions of units, and Riemannian structures [12, 13].

A manifold is an abstraction. Whereas manifolds like the sphere, the torus, and the surface of a pretzel are easy to comprehend as *submanifolds of Euclidean spaces*, other manifolds naturally arising in statistics have abstract descriptions (spaces of axes, spaces of shapes, etc); therefore, they have to be *embedded* into a numerical space  $\mathbb{R}^N$  for a better understanding. Whitney showed that any smooth  $d$ -dimensional manifold can be embedded in  $\mathbb{R}^{2d+1}$ . A manifold that is embedded in  $\mathbb{R}^N$  naturally inherits a Riemannian structure (infinitesimal arc length). Therefore, an embedded manifold automatically inherits two distances : a *chord distance* and a *Riemannian distance*. The pioneers of differential geometry (Gauss, Riemann, Cartan) considered geometric properties of a surface, a 2D manifold that is embedded in the Euclidean space, to be *extrinsic* if they are derived from the chord distance and *intrinsic* if they are derived from the restriction of the infinitesimal chord distance, also known as infinitesimal geodesic or arc distance. Following the classics, a Fréchet statistic (mean, mean set, total variance, etc) associated with a random sample on a manifold  $\mathcal{M}$  is said to be an *extrinsic statistic* (mean, mean set, total variance, etc) if the distance on the manifold is the chord distance associated with an embedding of the manifold in  $\mathbb{R}^N$ . Respectively, a Fréchet statistic associated with a manifold  $\mathcal{M}$  is said to be an *intrinsic*

*statistic (mean, mean set, total variance, etc)* if the distance on the manifold is the geodesic distance associated with the induced Riemannian structure on that manifold. Intrinsic and extrinsic means on abstract manifolds were first defined by Patrangenaru [18], who extended the notion of the mean of a distribution on a sphere or on a real projective space, using the method of center of mass and the method of moments of inertia in directional data analysis due to Watson [1]. Means of random vectors on submanifolds, as defined by Hendricks and Landsman [15], are extrinsic means.

Note that Riemannian structures on an abstract manifold can be also obtained via a partition of the unity, leading to the following question: are there Riemannian manifolds that cannot be isometrically embedded in some Euclidean space? The answer to this question is *negative* and is due to J. F. Nash [16], who considered this result more important than his others achievements for which he was awarded the Nobel Prize in Economics. Moreover, any homogeneous Riemannian manifold, and in particular any symmetric space, can be equivariantly embedded in a Euclidean space [17], showing that there are both infinitely many extrinsic means, as well as infinitely many intrinsic means that can be associated with a probability measure on a manifold, even on a homogeneous space, given the metric classification of Riemannian homogeneous spaces [18, 19].

Despite all the above, many years after the well-established isometric embedding theorem of Nash, confusion seems to persist in some circles about the roles of extrinsic and intrinsic means in statistics. It is sometimes argued that intrinsic analysis, based on *the* Riemannian distance, is to be preferred to extrinsic analysis because the latter is based on an arbitrary embedding among infinitely many possible embeddings [20]. The implication in this argument that there is a unique Riemannian metric tensor on a manifold is, of course, false; indeed, there are in general infinitely many metric tensors on a manifold. The argument of a unique Riemannian metric on a manifold was nevertheless taken at face value by many computational scientists, who for the reason of the ‘uniqueness’ only, would prefer running an intrinsic mean data analysis, no matter how impractical that would be. The erroneous idea that intrinsic means (or their local version, *Karcher means* [21]) are ‘more important’ has made swift gains among large segments of electrical engineers, computer scientists, and statisticians. As our arguments above show, other things being equal, intrinsic and extrinsic means have comparable theoretical statures for statistical inference. *But other things are not equal!* Unfortunately, there are no verifiable general criteria for the existence of (a unique) intrinsic mean, excepting those requiring a small support of the underlying distribution [22, 23]. Even in the case of the circle  $S^1$ , there is no simple broad criterion for uniqueness (Bhattacharya University of Arizona, Tucson, Arizona, USA, unpublished results). It is worth mentioning that when distributions have small support, intrinsic and extrinsic sample means are generally undistinguishable [6, 11, 24].

Intrinsic means inherit all the poor properties of arbitrary Fréchet means, and their computation is very slow, making them unhelpful in data analysis on manifolds. Karcher means have the additional disadvantage that their sample counterparts depend on the choice of the initial point in the computational algorithm and the algorithm may converge to a critical point of the Fréchet function that is not the intrinsic mean. For example, such an algorithm may converge even to a point of maximum of the Fréchet function.

By contrast, the necessary and sufficient condition for the existence of the extrinsic mean of random object  $X$  on a manifold  $\mathcal{M}$  embedded via  $j : \mathcal{M} \rightarrow \mathbb{R}^N$  is that the mean vector of  $j(X)$  is a *nonfocal* point of  $j(\mathcal{M})$  [10]. Also, extrinsic means can be computed easily.

One should note, though, that in physics there are sometimes considerations of mechanics that dictate the use of a particular metric tensor and the corresponding intrinsic mean. But this is almost never the case in statistics, where the main problem is discrimination among different distributions.

### 3. Data analysis examples

Throughout the remainder of the paper, we present examples of various types of data analysis on manifolds. In this section, for each type of data analysis, a methodology is described for the calculation of an extrinsic mean and that for an intrinsic mean, for that type of data. Examples of computations are then performed using both methodologies for a given sample and are presented with the required computational time. For timing purposes, all computations were performed using MATLAB on a machine running Windows XP on an Intel Core 2 Duo (Intel Corporation, Santa Clara, CA, USA) processor running at 2.33 GHz. We present these examples as support for using *extrinsic* statistics to perform visual quality control analysis for manufacturing processes.

#### 3.1. Spherical data

We first consider spherical data analysis. In general, given a random object  $X$  on a manifold  $\mathcal{M}$  and an embedding  $J : \mathcal{M} \rightarrow \mathbb{R}^N$ , if the mean vector  $\mu = E(J(X))$  is a nonfocal point of  $J(\mathcal{M})$ , then the extrinsic mean is  $\mu_E = J^{-1}(P_J(\mu))$ , where  $P_J$  is the projection on  $J(\mathcal{M})$ . In particular, given a random vector  $X$  on the unit sphere  $S^p \subset \mathbb{R}^{p+1}$ ,  $X^T X = 1$ , and the extrinsic mean is  $\mu_E = (1/\|E(X)\|)E(X)$ . For the purposes of this paper, we are

interested in the case  $p = 2$ . For observations  $x_1, \dots, x_n \in S^2$ , the extrinsic sample mean  $\hat{\mu}_E$  is calculated using the following formula:

$$\hat{\mu}_E = \frac{\bar{x}}{\|\bar{x}\|}, \quad (2)$$

where  $\bar{x}$  is the usual Euclidean mean and  $\|\cdot\|$  is the standard norm. This mean is based upon the chord distance between points. For observations  $x_1, \dots, x_n \in S^2$ , the intrinsic sample mean  $\hat{\mu}_I$  is the minimizer of the following Fréchet function:

$$F(p) = \sum_{i=1}^n d^2(x_i, p), \quad (3)$$

where  $d(x, y)$  is the arc distance between points  $x$  and  $y$ . There is no closed-form solution for the intrinsic mean. Instead, an iterative algorithm must be used. Such an algorithm is given as follows:

1. Make an initial estimate  $\tilde{\mu}_I$  of  $\hat{\mu}_I$ ; that is, use  $\hat{\mu}_E$
2. For each  $x_i$ , compute

$$v_i = u_i * \arccos \frac{x_i \tilde{\mu}_I^T}{\sqrt{u_i u_i^T}},$$

where  $u_i = x_i - (x_i \tilde{\mu}_I^T) \tilde{\mu}_I$

3. Compute  $\bar{v}$  and update  $\tilde{\mu}_I$  in the following manner:

$$\tilde{\mu}_{I, \text{new}} = \cos(\epsilon \sqrt{\bar{v} \bar{v}^T}) \tilde{\mu}_I + \sin(\epsilon \sqrt{\bar{v} \bar{v}^T}) \frac{\bar{v}}{\sqrt{\bar{v} \bar{v}^T}},$$

where  $\epsilon > 0$ .

4. Repeat until  $\sqrt{\bar{v} \bar{v}^T} < \epsilon$ .

To illustrate these computations and the time required to perform such tasks, we consider a set of wind direction data from Fisher *et al.* [2, p. 308]. The data consist of 29 observations and is provided as pairs of colatitude and longitude. Figure 4 displays these data on  $S^2$  in four views.

The extrinsic and intrinsic means were calculated using the methods described above and are shown in Figure 5, although in order to calculate the extrinsic mean, it was first necessary to convert to Cartesian coordinates. Additionally, the Fréchet function of which the intrinsic mean is the minimizer is displayed for a grid of values of colatitude and longitude in Figure 5. The amount of time required to compute  $\hat{\mu}_E$  was  $9.531 \times 10^{-5}$  s. The amount of time required to compute  $\hat{\mu}_I$  was 10.88 s.

To further illustrate the disparity in computational cost, we consider the calculation of bootstrap means. With the same methodology used previously, 200 resamples were taken and both types of means were obtained for each. To obtain the bootstrap means, as displayed in Figure 6, we applied the methodology again on the sample of means. For the extrinsic mean, the computational time required was 0.016762 s. For the intrinsic mean, the computational time required was 1572 s.

### 3.2. 3D size-and-shape data

We now consider data for which we are interested in analyzing both the shape and size of objects. For such data, each observation is represented as a  $k$ -ad, an ordered set of  $k$  points. A  $k$ -ad in  $\mathbb{R}^p$  is said to be in general position if the  $k$ -ad spans  $\mathbb{R}^p$ . For our purposes, we consider the case that  $p = 3$ .

Let  $\{\mathbf{x}_1, \dots, \mathbf{x}_n\}$ , where  $\mathbf{x}_j = (x_j^1, \dots, x_j^k)$ ,  $j = 1, \dots, n$ , be a sample of  $k$ -ads in general position in  $\mathbb{R}^3$ . The *extrinsic sample mean reflection size and shape* is  $[\bar{x}]_E = [\hat{\xi}]_{RS}$ , where  $\hat{\xi}$  is given by the eigenvectors corresponding to the three largest eigenvalues of

$$\hat{C} = \frac{1}{n} \sum_{j=1}^n \xi_j^T \xi_j$$

assuming that  $\hat{\lambda}_3$  is strictly greater than  $\hat{\lambda}_4$ , where  $\hat{\lambda}_1 \geq \dots \geq \hat{\lambda}_k$  are the eigenvalues of  $\hat{C}$  and  $\xi_j = x - \bar{x}$  [25]. If  $\hat{\lambda}_3 = \hat{\lambda}_4$ , which occurs with probability 0, then there is no unique extrinsic mean.

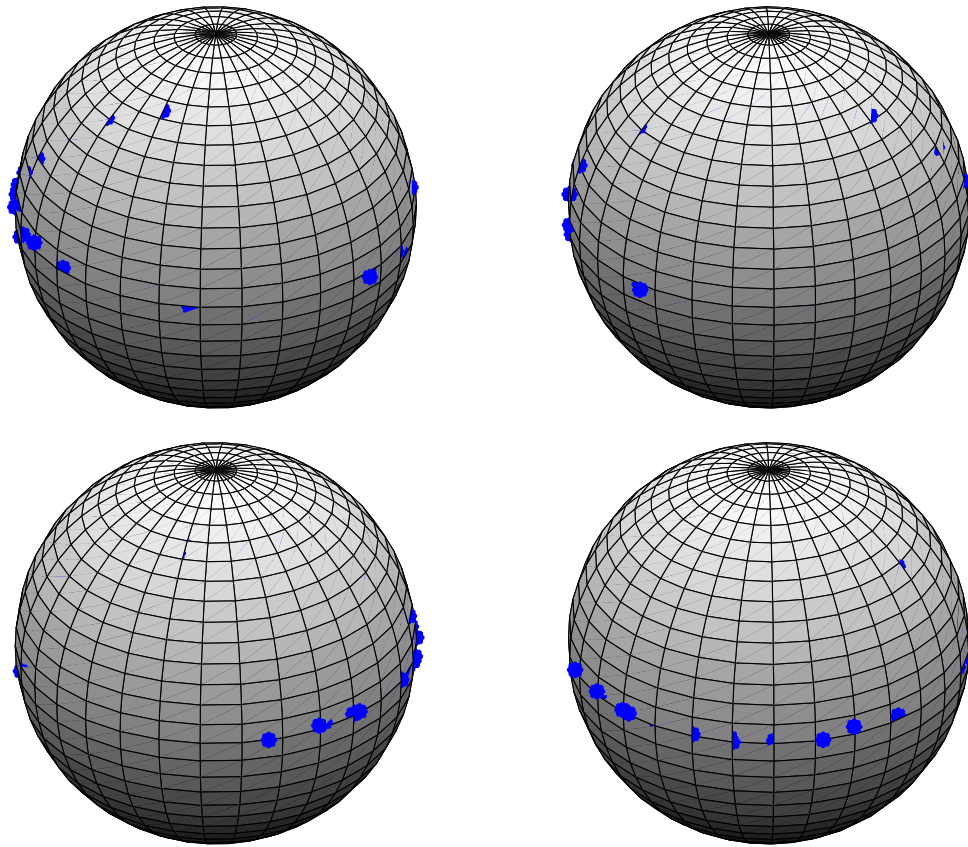


Figure 4. The wind direction data used for the computations.

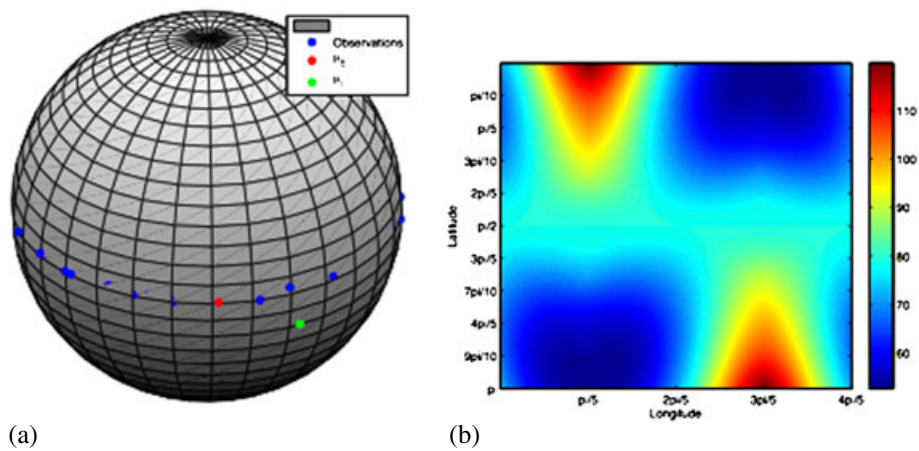


Figure 5. (a) The extrinsic and intrinsic means for the data. (b) The Fréchet function using arc distance as a function of colatitude and longitude.

The intrinsic sample mean size and shape  $\hat{\mu}_I$  is the minimizer of the following Fréchet function:

$$F(p) = \sum_{i=1}^n d^2(x_i, p) = \sum_{i=1}^n \inf_{\Gamma_i \in SO(3)} \|p - x_i \Gamma_i\|^2, \quad (4)$$

where  $\|\cdot\|$  is the standard norm in  $\mathbb{R}^3$  and  $\Gamma_i$  is a special orthogonal matrix. As with the spherical data, there is no closed-form solution for the intrinsic mean size and shape. Instead, the following iterative algorithm is used [5]:

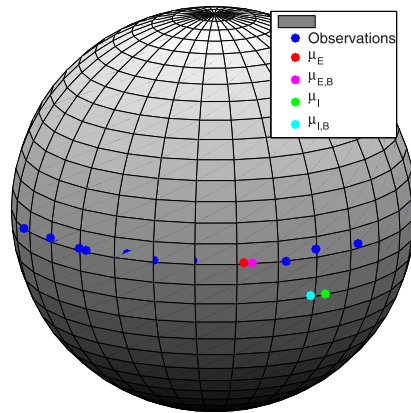


Figure 6. The extrinsic and intrinsic bootstrap means for the data compared with the extrinsic and intrinsic means.

1. Make an initial estimate  $\tilde{\mu}_I$  of  $\hat{\mu}_I$ ; that is, use  $\hat{\mu}_E$
2. For each  $\mathbf{x}_i$ , find the optimal ‘rotation’ matrix  $\Gamma_i$  using Procrustes alignment and compute

$$V_i = \xi_i \Gamma_i - \tilde{\mu}_I, \quad (5)$$

3. Compute  $\bar{V}$  and update  $\tilde{\mu}_I$  in the following manner:

$$\tilde{\mu}_{I,\text{new}} = \tilde{\mu}_I + \epsilon \bar{V}, \quad (6)$$

where  $\epsilon > 0$ .

4. Repeat until  $\|\bar{V}\| < \epsilon$ .

To demonstrate, we performed the above computations for a data set consisting of four protein active sites. The active sites, obtained from the RCSB Protein Data Bank and shown in Figure 7, are found in the proteins 1phf, 1phg, 2cpp, and 1m85 and bind to the ligand heme. As shown in Figure 8, the extrinsic mean size and shape, obtained after atoms matching, is visually indistinguishable from the intrinsic mean size and shape.

To detail the computational speeds of the two types of analysis, we computed bootstrap means similarly to the wind direction data. To examine the effect of sample size on the computational cost, we performed these calculations for samples of size 4, 5, 6, 8, 12, and 16. For the samples of size greater than 4, the observed data were simulated on the basis of the original sample. The times, in seconds, required for these computations are shown in Table I. Increasing the sample size has no significant effect on the computational cost for calculating the extrinsic mean size and shape. However, increasing the sample size has a large effect on the computational cost for calculating the intrinsic mean size and shape.

### 3.3. Direct similarity shapes of planar contours

In this section, we consider data analysis of planar contours; for more details on contour data analysis, see Ellingson *et al.* [26]. Traditionally, such data are discretized, and each curve is represented as a  $k$ -ad, where each landmark on the curve is a point in  $\mathbb{C}$ . Let  $\xi_1, \dots, \xi_n$  be a sample of centered  $k$ -ads. The Veronese–Whitney extrinsic sample mean shape is the unit eigenvector corresponding to the largest eigenvalue of  $\sum_{i=1}^n (1/\|\xi_i\|^2) \xi_i \xi_i^*$  assuming that the largest eigenvalue is simple.

The recently developed elastic framework for shape analysis of planar curves instead utilizes functional representation for such data and utilizes intrinsic analysis [27]. As with the previously discussed types of data, there is no closed form for the intrinsic mean shape, so an iterative algorithm similar in concept to that used for the wind direction data must be used to perform computations.

Computations for both approaches were performed on a sample of four observations of contours of the ‘1’ hand gesture, shown in Figure 9. To illustrate the difference in computational cost, we computed 95% bootstrap confidence intervals for both the extrinsic mean shape and the intrinsic mean shape using 400 resamples and 300 randomly chosen landmarks. These confidence regions are shown in Figure 10. For the extrinsic mean shape, these calculations required 48 s to complete. However, for the intrinsic mean shape, these calculations required 47.9 h.

As a second example, these methods were also performed on a sample of four observations of contours of dogs, which is shown in Figure 11. Again, 95% bootstrap confidence regions were computed for both approaches, using 300 resamples,

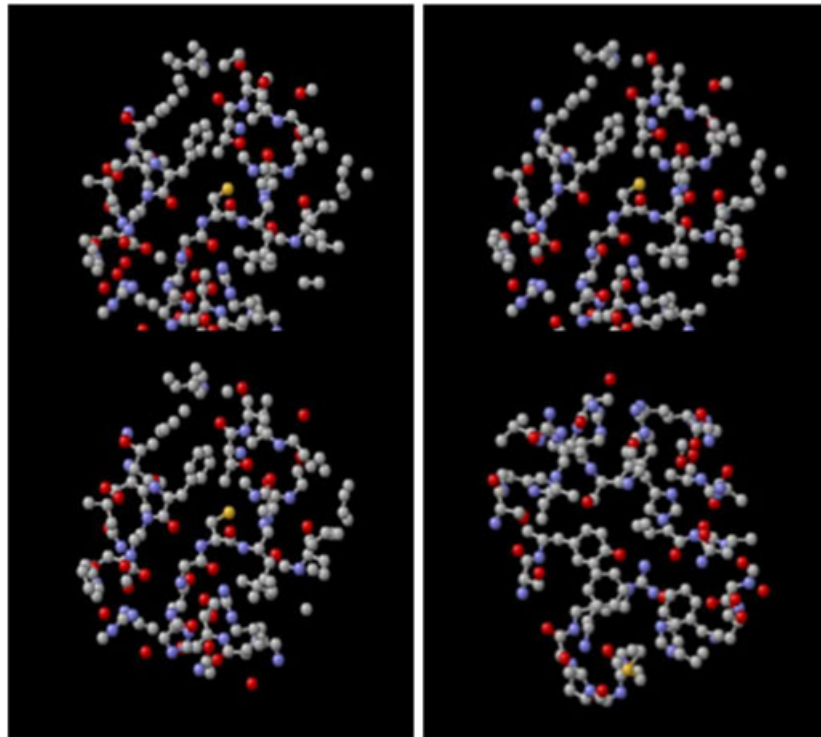


Figure 7. Active sites that bind to heme for proteins 1phf, 1phg, 2cpp, and 1m85.

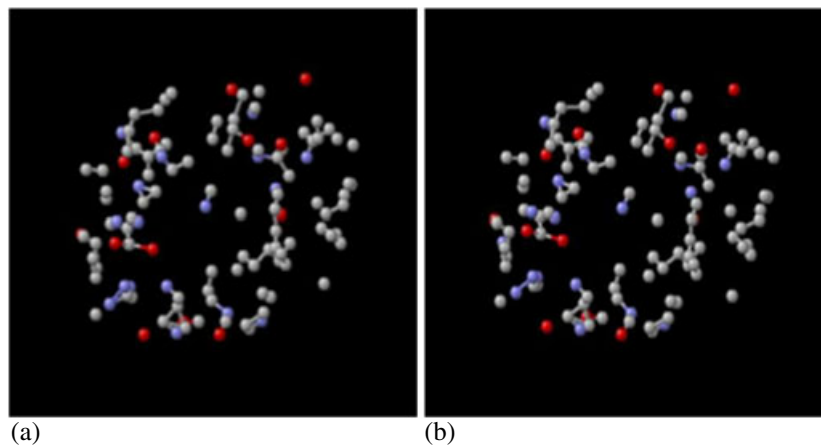


Figure 8. (a) The Schoenberg extrinsic mean reflection size and shape and (b) the intrinsic mean size and shape of atoms common to the active sites.

<b>Table I.</b> The times required to compute the mean size and shape for various sample sizes.			
Sample size	Extrinsic	Intrinsic	Ratio
4	15.9	29.3	1.84
5	15.3	32.0	2.09
6	15.2	36.2	2.38
8	14.8	60.2	4.07
12	15.3	92.1	6.01
16	16.5	123.6	7.49

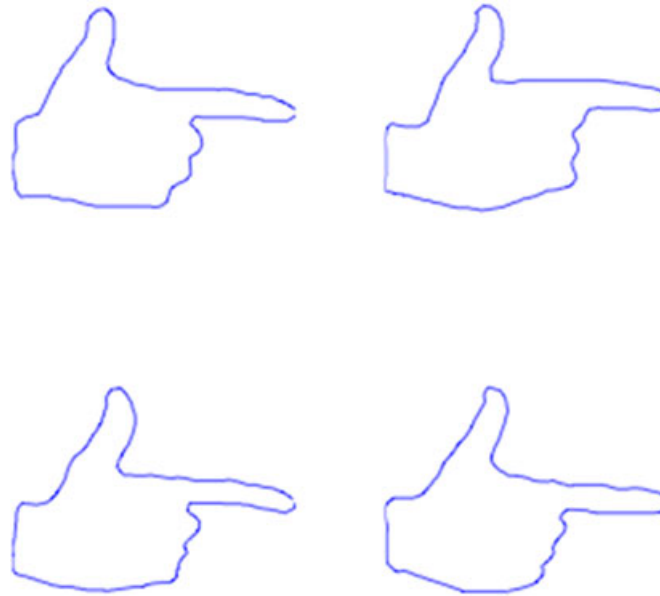


Figure 9. Four observations of contours of the '1' hand gesture.

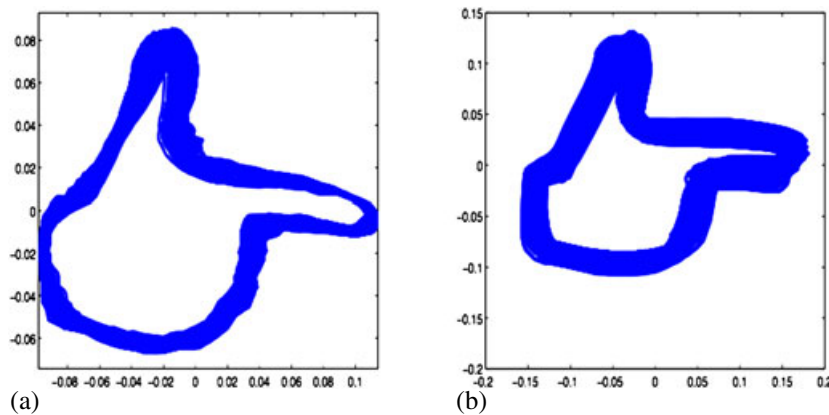


Figure 10. Bootstrap 95% confidence regions using 400 resamples for (a) the extrinsic mean shape of the '1' hand gesture and (b) the intrinsic mean shape of the '1' hand gesture.

where each contour is provided as 100 evenly spaced landmarks. These confidence regions are shown in Figure 12. For the extrinsic mean shape, these calculations required 5.6 s to complete. However, for the intrinsic mean shape, these calculations required 8.9 h.

### 3.4. Projective shapes

*Projective shape spaces* can be identified with direct products of projective spaces. Therefore, projective shape analysis can be reduced to a multivariate axial data analysis. Our example in the area of face recognition is based on data from the live BBC program 'Tomorrow's World' Figure 13. The example was introduced in [28]. Six almost coplanar landmarks (ends of eyes plus ends of lips) have been recorded from 14 digital images of the same person (an actor posing in different disguises). Face appearance in these pictures may be neither frontal nor lateral. Mardia and Patrangenaru [28] showed that, given that the landmark configuration is almost planar, the frontal views and the one quarter view yield the same extrinsic mean projective shape (Figures 12 and 13).

In [29], coordinates of two additional landmarks have been recorded ('bridge of the nose' and 'tip of the nose'). The eight landmarks considered are significantly not coplanar as shown by Balan *et al.* (2009) [30]; therefore, a 3D projective shape analysis is more appropriate for this configuration. If one compares the nonparametric bootstrap distributions of the extrinsic sample mean 2D projective shape of a configuration of five points, in one-quarter views versus frontal views of

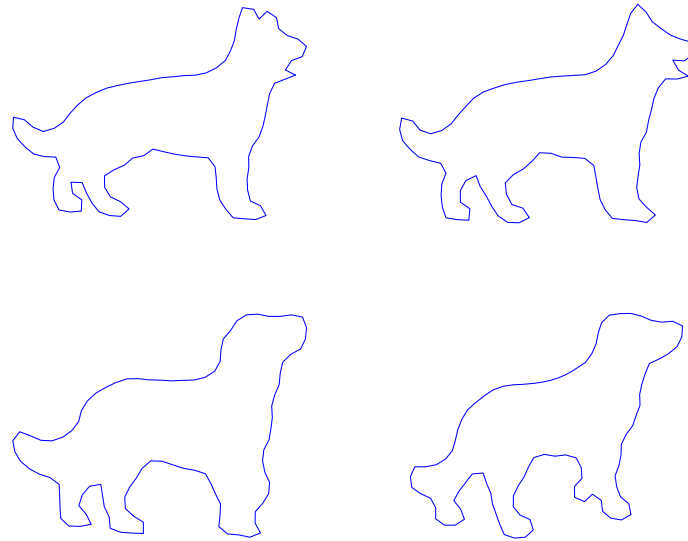


Figure 11. Four observations of contours of a side view of a dog.

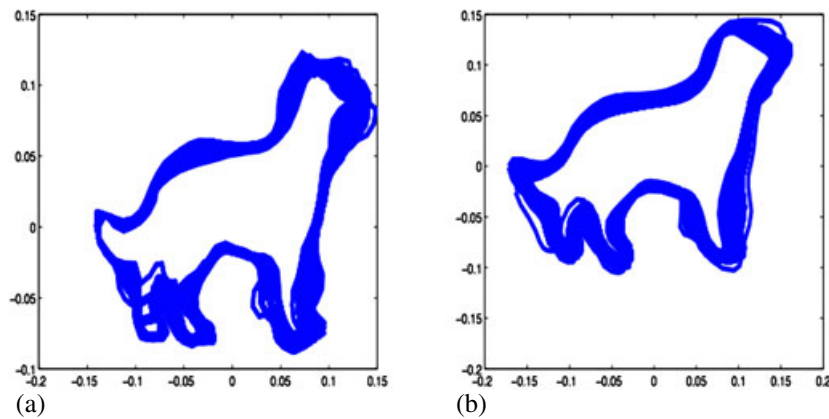


Figure 12. Bootstrap 95% confidence regions using 400 resamples for (a) the extrinsic mean shape of the four dogs and (b) the intrinsic mean shape of the four dogs.



Figure 13. BBC data: 14 views of an actor face.

the actor, we notice that even for configurations that are close to coplanar, these regions have only a small overlap. In Figure 14, one may notice this effect, thus showing the limitations of the 2D shape analysis for face recognition.

Given that  $\mathbb{R}P^d$  inherits a Riemannian structure of constant curvature from the round sphere, by identifying antipodal points, for relatively concentrated data, computations of *intrinsic sample means on real projective spaces are identical with those for spherical data*. Bootstrapping the intrinsic sample means on the real projective space takes too long to be considered here (expect more than one day for 100 resamples with repetition from the wind direction data).

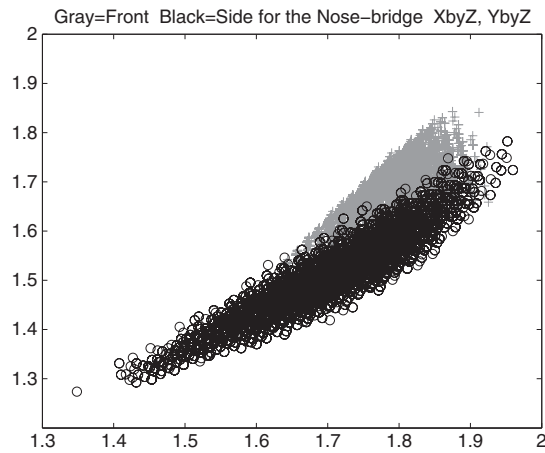


Figure 14. Affine views of the bootstrap distribution of the extrinsic mean axial coordinate corresponding to the bridge of nose landmark. Frontal views = +. One-quarter views = o.

#### 4. Applications to quality control

With the use of extrinsic statistics over intrinsic statistics for data analysis on a number of manifolds having been motivated, this section presents two applications for the use of extrinsic analysis in the visual quality control of manufacturing processes. Both examples are in the area of projective shape analysis and perform hypothesis tests to check for defects in a manufactured object.

The first application follows from the methodology used by Patrangenaru [31]. Consider a manufactured object whose surface is designed to be flat. The flatness of this surface can be studied using 2D projective shape analysis after taking a number of photographs of the scene. The coordinates of a number of evenly spread points are recorded from the surface of the object, and their projective coordinates are registered with respect to a convenient projective frame. A *projective frame* in plane is an ordered set of four points in general position, so four points are selected for this purpose (e.g., the corners of the surface). If the surface is perfectly flat, the projective shape is independent of the camera positions; therefore, ideally, its extrinsic total variance  $t\Sigma_E$  of the projective shape is zero (for details on the total extrinsic variance, see Bhattacharya and Patrangenaru [32]). This corresponds to testing the following hypothesis:

$$H_0 : t\Sigma_E = 0 \text{ vs. } H_1 : t\Sigma_E \neq 0. \quad (7)$$

A rejection of the null hypothesis would indicate the likely presence of a blemish, resulting in the surface not being flat.

A second application uses extrinsic statistics for 3D projective shape analysis and follows from an example presented by Patrangenaru *et al.* (2010) [29]. For simplicity, in our toy example, we consider the manufacturing of a 3D polyhedral object according to a blueprint displayed in Figure 15. If an object were constructed correctly according to this blueprint, it would consist of three cubes that sit on the top of each other, whose sides from top to bottom are four, six and ten units in length. However, we consider an object that instead has a top cube with sides five units in length. Figure 16 displays a digital image of this object with visible corners, taken as landmarks, numbered from 1 to 19.

Sixteen randomly selected photographs of this object, each showing all of the selected landmarks, were paired into eight pairs of images, as displayed in Figure 17, which were then used to obtain eight 3D projective reconstructions of the object [33, p. 121]. The projective shapes of these reconstructed configurations can be regarded as random objects on the projective shape space due to camera distortion and computational errors in the landmark selection and reconstruction processes. Landmarks 8, 12, 17, 18, and 19 were chosen, in this order, to form a projective frame in 3D. With respect to this frame, the projective coordinates of the other landmarks yield a sample of points in the projective shape space  $P\Sigma_3^{19} = (\mathbb{R}P^3)^{14}$ , where each point represents a projective shape. The extrinsic sample mean of the eight projective shapes was computed following the work of Patrangenaru *et al.* [29].

Checking whether the object was constructed according to the blueprint is equivalent to testing the following hypotheses:

$$H_0 : \mu_{j_{19}} = \mu_0 \text{ vs. } H_1 : \mu_{j_{19}} \neq \mu_0, \quad (8)$$

where  $\mu_0$  is the projective shape of the blueprint and  $\mu_{j_{19}}$  is the extrinsic mean projective shape of random 3D reconstructions of the object. Simultaneous Bonferroni confidence intervals can be used to perform this test. Unlike in the work of

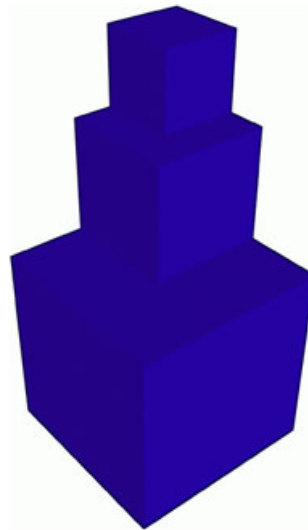


Figure 15. 3D blueprint for a configuration of blocks.

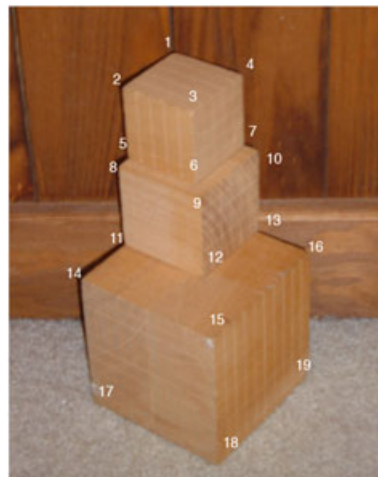
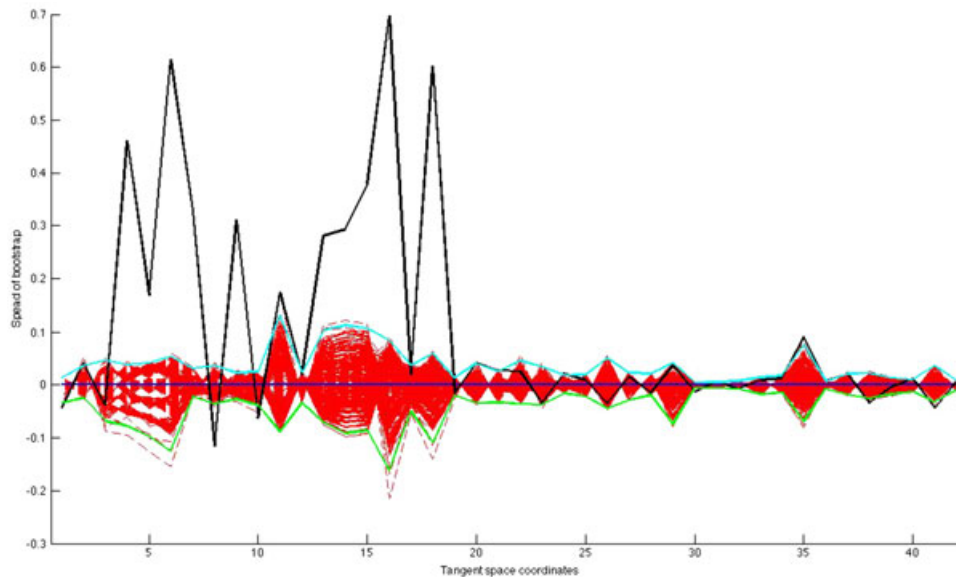


Figure 16. The 19 landmarks displayed are used for 3D scene reconstruction and statistical analysis.



Figure 17. Sixteen digital camera views of a 3D object modified from the blueprint. The images from the top row are paired with the images in the bottom row for reconstruction.



**Figure 18.** Ninety percent simultaneous confidence intervals for the tangential coordinates of bootstrap sample mean projective coordinates of 14 landmarks not used as the projective frame. Every three successive coordinates correspond to one landmark. The extrinsic sample mean is represented by the dark blue line. The red lines correspond to the bootstrap extrinsic sample means. The light blue and green lines represent the confidence limits. The coordinates corresponding to the blueprint are represented by the black line.

Patrangenaru *et al.* [29], where pivotal statistics were used for the 14 marginal axial distributions, here we use 42 nonpivotal confidence intervals for their coordinates. The advantage is that the nonpivotal method avoids computing the extrinsic sample covariance matrix and its inverse; therefore, it is computationally faster. To achieve a reliable conclusion, 1000 resamples with repetition were used.

For the rejection of  $H_0$ , it suffices to show that one coordinate of the blueprint for one of the landmarks falls outside the corresponding bootstrap confidence interval. Figure 18 shows the 90% simultaneous confidence intervals for the 14 landmarks not utilized in the projective frame, using coordinates in the tangent space of the extrinsic sample mean. Each landmark is represented by three successive tangent space coordinates, so the seven landmarks of the top block corresponds to coordinates 1 through 21. Landmarks 2, 3, 5, and 6 of the blueprint are substantially outside of their respective confidence intervals. This provides sufficient evidence to reject the null hypothesis. Because the top block of the object was not selected to the blueprint specifications, this is the correct decision. It should be noted that the coordinates for the remaining landmarks of the object fall within the confidence intervals or just slightly outside, as expected, because the middle and bottom blocks were constructed according to the blueprint. This is advantageous because, not only does this approach check if the projective shape of an object matches a blueprint, but it also determines which landmarks likely correspond to defects.

## 5. Summary and conclusions

Much of modern data analysis consists of problems involving data on manifolds. Among the fields in which such data occurs are medical imaging, directional data analysis, pattern recognition, and visual quality control. For a statistical analysis on this data, either extrinsic or intrinsic analysis may be used.

The computational cost of performing extrinsic analysis on manifold data is substantially less than the computational cost of performing intrinsic analysis on the same data. This is especially noticeable when working with large data sets and/or performing analysis requiring large numbers of repetitions, as with nonparametric bootstrap techniques. As shown with the protein data, in many cases, the extrinsic and intrinsic means are indistinguishable from each other despite the difference in computational time, providing strong support for the use of extrinsic analysis in such situations.

In other scenarios, one must look to the requirements for the application at hand. For instance, extrinsic means exist outside a negligible singular set, whereas intrinsic means are not, in general, guaranteed to exist. Furthermore, for a given embedding  $J$ , the extrinsic mean is the projection on  $J(\mathcal{M})$ , but there is no natural description of the intrinsic mean. Because these considerations, extrinsic analysis is often preferable for statistical analyses.

## Acknowledgements

We would like to thank the editor and the referees for suggestions that helped improve the manuscript and Frits H. Ruymgaart and Jinfeng Zhang for discussions on related joint projects. This research was supported by the National Science Foundation Grants DMS-0805977, DMS-0806011, NSF-DMS-0713012 and the National Security Agency Grant MSP-H98230-08-1-005.

## References

1. Watson G. *Statistics on Spheres*, University of Arkansas Lecture Notes in the Mathematical Sciences, Vol. 6. John Wiley and Sons, Inc.: New York, 1983.
2. Fisher N, Lewis T, Embleton B. *Statistical Analysis of Spherical Data*. Cambridge University Press: Cambridge, 1987.
3. Beran R, Fisher N. Nonparametric comparison of mean axes. *Annals of Statistics* 1998; **26**:472–493.
4. Bookstein F. *The Measurement of Biological Shape and Shape Change*, Vol. 24. Springer: New York, 1978.
5. Dryden I, Mardia K. *Statistical Shape Analysis*. Wiley: New York, 1998.
6. Bhattacharya R, Bhattacharya A. Statistics on manifolds with applications to shape spaces. *Perspectives in Mathematical Sciences I: Probability and Mathematics*, Narasimha Sastry NS, Rao TSSRK, Delampady M, Rajeev M (eds). Indian Statistical Institute: Bangalore, 2009; 41–70.
7. Crane M, Patrangenaru V. Random change on a lie group and mean glaucomatous projective shape change detection from stereo pair image. *Journal of Multivariate Analysis* 2011; **102**(2):225–237.
8. Fréchet M. Les éléments aléatoires de nature quelconque dans un espace distancié. *Annales de l'Institut Henri Poincaré* 1948; **10**:215–310.
9. Ziezold H. On expected figures and a strong law of large numbers for random elements in quasi-metric spaces. *Transactions of the Seventh Prague Conference on Information Theory, Statistical Decision Functions, Random Processes and of the Eighth European Meeting of Statisticians*. Reidel: Dordrecht, 1977; 591–602.
10. Bhattacharya RN, Patrangenaru V. Large sample theory of intrinsic and extrinsic sample means on manifolds—I. *Annals of Statistics* 2003; **31**(1):1–29.
11. Bhattacharya RN, Patrangenaru V. Large sample theory of intrinsic and extrinsic sample means on manifolds—part II. *Annals of Statistics* 2005; **33**(3):1211–1245.
12. Spivak M. *A Comprehensive Introduction to Differential Geometry*, 2nd edition, Vol. I–II. Publish or Perish, Inc.: Wilmington, Delaware, 1979.
13. Kobayashi S, Nomizu K. *Foundations of Differential Geometry*, Vol. I, II. Wiley Classics Library: New York, 1996. Reprint of the 1963–1969 original.
14. Patrangenaru V. Asymptotic statistics on manifolds, *PhD dissertation*, Indiana University, 1998.
15. Hendriks H, Landsman Z. Mean location and sample mean location on manifolds: asymptotics, tests, confidence regions. *Journal of Multivariate Analysis* 1998; **67**:227–243.
16. Nash J. The imbedding problem for Riemannian manifolds. *Annals of Mathematics* 1956; **63**(2):20–63.
17. Moore JD. Equivariant embeddings of Riemannian homogeneous spaces. *Indiana University Mathematics Journal* 1976; **25**:271–279.
18. Patrangenaru V. Locally homogeneous Riemannian manifolds and Cartan triples. *Geometriae Dedicata* 1994; **50**:143–164.
19. Patrangenaru V. Classifying 3 and 4 dimensional homogeneous Riemannian manifolds by Cartan triples. *Pacific Journal of Mathematics* 1996; **173**:511–532.
20. Srivastava A, Klassen EP. Monte Carlo extrinsic estimators for manifold-valued parameters. *IEEE Transactions on Signal Processing* 2002; **50**:299–308.
21. Srivastava A, Klassen EP. Bayesian and geometric subspace tracking. *Advances in Applied Probability(SGSA)* 2004; **36**:43–56.
22. Karcher H. Riemannian center of mass and mollifier smoothing. *Communications on Pure and Applied Mathematics* 1977; **30**:509–554.
23. Kendall DG, Barden D, Carne TK, Le H. *Shape and Shape Theory*. Wiley: New York, 1999.
24. Bhattacharya RN, Bhattacharya A. Nonparametric statistics on manifolds with applications to shape spaces. *Pushing the Limits of Contemporary Statistics: Contributions in Honor of J. K. Ghosh*, Clarke B, Ghosal S (eds), IMS Collection 3. Institute of Mathematical Statistics: Berchwood, Ohio, 2008.
25. Bandulasiri A, Bhattacharya RN, Patrangenaru V. Nonparametric inference for extrinsic means on size-and-(reflection)-shape manifolds with applications in medical imaging. *Journal of Multivariate Analysis* 2009; **100**:1867–1882.
26. Ellingson L, Ruymgaart F, Patrangenaru V. Nonparametric estimation for extrinsic mean shapes of planar contours. *Technical Report M99*, Department of Statistics, Florida State University, 2010.
27. Joshi S, Srivastava A, Klassen E, Jermyn I. Removing shape-preserving transformations in square-root elastic (SRE) framework for shape analysis of curves. *Workshop on Energy Minimization Methods in CVPR (EMMCVPR)*, August 2007.
28. Mardia KV, Patrangenaru V. Directions and Projective Shapes. *Annals of Statistics* 2005; **33**:1666–1699.
29. Patrangenaru V, Liu X, Sugathadasa S. Nonparametric 3D projective shape estimation from pairs of 2D images—I, in Memory of W.P. Dayawansa. *Journal of Multivariate Analysis* 2010; **101**:11–31.
30. Balan V, Crane M, Patrangenaru V, Liu X. Projective shape manifolds and coplanarity of landmark configurations. A nonparametric approach. *Balkan Journal of Geometry and Its Applications* 2009; **14**(1):1–10.
31. Patrangenaru V. New large sample and bootstrap methods on shape spaces in high level analysis of natural images. *Communications in Statistics—Theory and Methods* 2001; **30**(8 & 9):1675–1693.
32. Bhattacharya RN, Patrangenaru V. Nonparametric estimation of location and dispersion on Riemannian manifolds. *Journal of Statistical Planning and Inference* 2002; **108**:23–35.
33. Ma Y, Soatto S, Kosecka J, Sastry SS. *An Invitation to 3-D Vision*. Springer: New York, 2006.